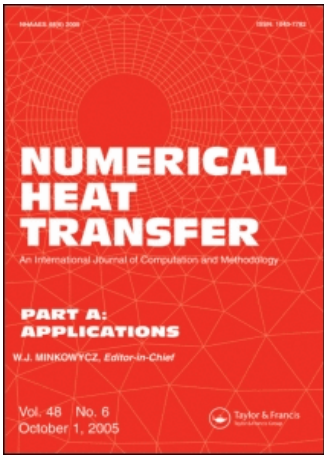

Numerical Heat Transfer, Part A: Applications
An International Journal of Computation and Methodology
Publication details, including instructions for authors and subscription information:
http://www.informaworld.com/smpp/title~content=t713657973

Modeling IC Engine Conjugate Heat Transfer Using the KIVA Code

Egel Urip [a]; Ka Heng Liew [a]; S. L. Yang [a]
[a] Department of Mechanical Engineering—Engineering Mechanics, Michigan Technological University, Houghton, Michigan, USA

Online Publication Date: 01 January 2007

To cite this Article: Urip, Egel, Liew, Ka Heng and Yang, S. L. (2007) 'Modeling IC Engine Conjugate Heat Transfer Using the KIVA Code', Numerical Heat Transfer, Part A: Applications, 52:1, 1 — 23

To link to this article: DOI: 10.1080/10407780601112803
URL: http://dx.doi.org/10.1080/10407780601112803

Numerical Heat Transfer, Part A, 52: 1–23, 2007

ISSN: 1040-7782 print/1521-0634 online
DOI: 10.1080/10407780601112803

Taylor & Francis
Taylor & Francis Group

MODELING IC ENGINE CONJUGATE HEAT TRANSFER USING THE KIVA CODE

Egel Urip, Ka Heng Liew, and S. L. Yang
Department of Mechanical Engineering—Engineering Mechanics, Michigan Technological University, Houghton, Michigan 49931, USA

Locating hotspots in metal engine components can be used as an impetus to design a better cooling system. This study focuses on a numerical investigation of a three-dimensional (3-D) transient heat transfer process for a Ford 5.4-L V8 engine. A 3-D transient finite-volume method to solve the heat conduction equation is presented first. This is followed by the implementation of the coupling equations at the gas–solid interface into the KIVA code. The numerical model is validated by a one-dimensional heat conduction problem. Finally, 3-D simulation of the Ford engine with conjugate heat transfer mode is presented and discussed.

INTRODUCTION

In internal combustion (IC) engines, an air–fuel mixture is the medium used to produce mechanical work through chemical reaction. For a typical four-stroke reciprocating engine, the mixture in the combustion chamber is compressed and then ignited, resulting in a tremendous increase of pressure and temperature. Pressure difference between the combustion chamber and the ambient forces the piston to move up and down, producing mechanical work. The second law of thermodynamics states that a certain amount of heat generated from the combustion must be rejected. Coolant is typically used in the engine cooling jacket as a medium to accommodate the heat rejection. An insufficient heat removal rate could result in higher thermal stress in the engine.

An improved cooling system can potentially reduce the amount of coolant needed and the thermal stress, resulting in a longer engine life. A smaller electronically controlled pump, which requires less power, can now be used to substitute for the old inefficient mechanical pump to improve engine efficiency. This can be accomplished by understanding the physical process occurring in the engine itself. Fast transient heat flux from the combustion to the cylinder liner, head, and piston surface and transient heat loss to the cooling passages are important factors affecting the heat transfer process in engines.

Received 20 June 2006; accepted 19 September 2006.

The authors would like to acknowledge the financial support of Visteon. The authors would also like to thank Dan Kapp and Thomas Veling of Ford Motor Company for providing us their F-150 CAD files.

Address correspondence to S. L. Yang, Michigan Technological University, Department of Mechanical Engineering—Engineeriong Mechanics, 1400 Townsend Drive, Houghton, MI 49931-1295, USA. E-mail: slyang@mtu.edu

NOMENCLATURE

B	5.5 in Eq. (12)
c_μ	0.09 for standard k–ε turbulence model, 0.085 for RNG k–ε turbulence model
C_P	specific heat
h	convective heat transfer coefficient
I	specific internal energy
K	turbulent kinetic energy
Pr_l	laminar Prandtl number
q	heat transfer rate
r	radius
RPR	reciprocal of the turbulent Prandtl number
t	time
T	temperature
V	volume
y	distance from the wall
κ	thermal conductivity or Karmann's constant in Eq. (12)
ρ	density
ν	thermal diffusitivity
ν_l	laminar kinematic viscosity of air
Φ_D	implicit parameter

Subscripts

f	fluid
l	laminar
L	element to the left of control surface
p	particle/parcel
R	element to the right of control surface
s, p	film surface temperature at the film–gas interface (in Figure 2)
∞	ambient

The 2001 Ford 5.4-L V8 260-HP naturally aspirated F-150 truck engine will be used as the engine model, and one of the cylinders will be modeled in this study. The KIVA 3 V Release 2 code, an open computational fluid dynamics (CFD) source code that solves transient three-dimensional (3-D) chemically reactive flows with sprays, will be used to simulate the in-cylinder flow. The transport equations of the gas flow in the code are discretized by the finite-volume method, which only recognizes hexahedron elements arranged in a block-structured manner [1–4].

A structured finite-volume method to model temperature distribution inside the metal engine components was previously developed and validated [5]. Further improvement had been added into the scheme, allowing it to model complex geometries such as the metal components inside the engine head. It is now based on an unstructured finite-volume method that permits combination of four different types of elements: tetrahedron, pyramid, prism, and hexahedron. The scheme has been implemented into the KIVA code, and the code is now capable of solving fluid (gas-phase) flow with conjugate heat transfer mode. At the gas–solid interface, pyramid, prism, or hexahedron elements can be used to transmit information from the structured fluid domain (the KIVA code) to the unstructured solid domain (this study).

Related research in the field of IC engine heat transfer has been reported in the past [6–8]. An important key difference lies in the method of treating heat transfer at the gas–solid interface. The above-cited references use two or more software tools to simulate the gas flow and the temperature distribution of the engine metal components. In the first step of their calculation, using either a constant uniform or a non-uniform wall temperature, a CFD code is used to obtain the heat flux history at the combustion chamber surface by solving the gas phase alone. The heat flux history is then used as a transient/cycle-averaged 3-D thermal boundary condition for the solution of the metal components temperature using a separate heat conduction program. The newly updated wall temperature is reused to update the gas-phase solution, and the whole procedure becomes a very tedious iteration [8]. It is noted

that the above approach uncouples the gas phase from the solid phase. Similar engine heat transfer studies using simple geometry and physical models have also been reported in the past [9–11].

In this study, however, the gas phase is coupled with the solid phase throughout the engine cycles. Thus a more accurate and realistic solution could be obtained. Because of the nature of moving piston, a periodic steady-state solution is expected, assuming ambient and engine operating conditions remain the same. A nonuniform initial condition, which is close to a periodic steady-state solution, must be used to obtain such a solution. This is difficult to put into practice, however, because most of the time, the solution is not available. Uniform initial conditions are instead used for both the gas and the solid domains. From our numerical experience, the gas flow and its properties will reach periodic or close to periodic steady state within two or three engine cycles, which is feasible to solve with today's computing power. In contrast, the temperature distribution inside the metal engine components will take many more engine cycles to achieve the periodic steady state, depending on thermal penetration depth [5,12] and thermal properties of the metal components, e.g., specific heat, thermal conductivity, and density. Running the KIVA code with conjugate heat transfer mode for so many engine cycles would require massive computing power. Thus an approach similar to the work described in the previous paragraph is also an option in the current investigation.

SOLID-PHASE ENERGY EQUATION

Transient heat conduction without internal heat generation is described by the following equation:

$$\frac{\partial(\rho I)}{\partial t} = \nabla \cdot (\kappa \nabla T) \tag{1}$$

Discretization of Eq. (1) closely resembles the KIVA code. Finite-volume technique is used for the spatial differencing for a number of control volumes or cells. The first-order Euler method is used to discretize the unsteady term, as was done in the KIVA code. Equation (1) assumes temperature dependence of specific heat and thermal conductivity. To proceed with the discretization, through the divergence theorem, the volume integral of Eq. (1) becomes

$$\rho \frac{\partial}{\partial \mathrm{t}} \int_{\mathrm{CV}} I \mathrm{dV} = \int_{\mathrm{CS}} \kappa \nabla T \cdot \mathrm{d}\vec{A} \tag{2}$$

where $\mathrm{d}\vec{A}$ is the outward normal area vector of control faces. Discretizing Eq. (2) in time and space gives

$$\rho V C_p^n \frac{T^{n+1} - T^n}{\Delta \mathrm{t}} \sum_m \kappa_m^n \nabla [(1 - \Phi_D) T^n + \Phi_D T^{n+1}]_m \cdot \vec{A}_m \tag{3}$$

The superscript n in Eq. (3) indicates time-level value, e.g., T^n represents temperature at time level n. Thermodynamics quantities, e.g., ρ, T, κ, and C_P, are

cell-centered quantities, and their values are uniform within a cell. The subscript m represents summation over all the control surfaces. It represents the surface integral in Eq. (2). For derivation purposes, the diffusion term of one of the control faces, say surface a, can be represented as

$$\kappa_a \nabla \mathrm{T_a} \cdot \vec{A}_a \tag{4}$$

Two elements meet at a common interface, called an interior face. Two possible interior faces, triangle and quadrilateral, are identified and will be used to explain how Eq. (4) is calculated, as illustrated in Figure 1. Let us define subscripts L and R for elements to the left and to the right of the control surface (CS) a. The diffusion term across the CS is calculated by

$$\kappa_a \nabla T_a \cdot \vec{A}_a = \kappa_a [B(T_R - T_L) + C(T_3 - T_1) + D(T_4 - T_2)] \tag{5a}$$

or

$$\kappa_a \nabla T_a \cdot \vec{A}_a = \kappa_a [B(T_R - T_L) + C(T_3 - T_{12}) + D(T_{13} - T_2)] \tag{5b}$$

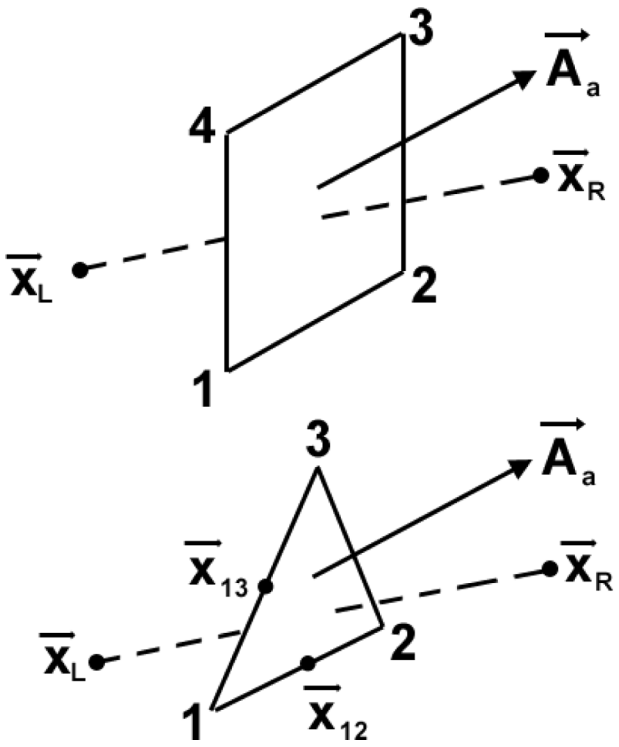

Figure 1. Two possible interior faces.

where

$$\kappa_a = \frac{\kappa_L + \kappa_R}{2} \tag{5c}$$

$\vec{x}_L$ and $\vec{x}_R$ are centers of cells and $\vec{x}_{12}$ and $\vec{x}_{13}$ are midway points between side 12 and side 13, respectively. $\vec{A}_a$ is the outward normal area vector of the CS. Coefficients B, C, and D are determined by solving

$$B(\vec{x}_R - \vec{x}_L) + C(\vec{x}_3 - \vec{x}_1) + D(\vec{x}_4 - \vec{x}_2) = \vec{A}_a \tag{6a}$$

or

$$B(\vec{x}_R - \vec{x}_L) + C(\vec{x}_3 - \vec{x}_{12}) + D(\vec{x}_{13} - \vec{x}_2) = \vec{A}_a \tag{6b}$$

T_L and T_R are temperatures of the two cells in question. T_1 is a node temperature obtained by a simple average of all cells touching node 1, and T_2, T_3, and T_4 are defined analogously. T_{12} is a midway temperature from linear interpolation of T_1 and T_2. Equations (5) and (6) are then performed analogously to the other control surfaces to obtain the total summation in Eq. (3).

It should be noted that Eqs. (5) and (6) could yield a less accurate solution for a multiple-medium domain with vastly differing thermal properties. An example for a typical IC engine application would be a sandwich arrangement of an aluminum engine head, head gasket, and cast-iron engine block. For applications that account for multiple-medium domains, equivalent coefficients in Eqs. (5) and (6) must be used to represent the physics correctly [13]. To accurately model heat transfer across a multiple-medium problem, two constraints are applied at the CS. For derivation purposes, the quadrilateral CS in Figure 1 is used for illustration.

$$(T_i)_L = (T_i)_R \tag{7a}$$

$$(q_i)_L = (q_i)_R \tag{7b}$$

$$(q_i)_L = \kappa_L[B_L(T_i - T_L) + C_L(T_3 - T_1) + D_L(T_4 - T_2)] \tag{7c}$$

$$(q_i)_R = \kappa_R[B_R(T_R - T_i) + C_R(T_3 - T_1) + D_R(T_4 - T_2)] \tag{7d}$$

and

$$B_L(\vec{x}_i - \vec{x}_L) + C_L(\vec{x}_3 - \vec{x}_1) + D_L(\vec{x}_4 - \vec{x}_2) = \vec{A}_a \tag{8a}$$

$$B_R(\vec{x}_R - \vec{x}_i) + C_R(\vec{x}_3 - \vec{x}_1) + D_R(\vec{x}_4 - \vec{x}_2) = \vec{A}_a \tag{8b}$$

Subscript i is the center of the CS. With some tedious algebraic derivations, one obtains

$$\kappa_a \nabla T_a \cdot \vec{A}_a = \kappa_e [B_e(T_R - T_L) + C_e(T_3 - T_1) + D_e(T_4 - T_2)] \tag{9a}$$

where subscripts e represent equivalent coefficients at surface a:

$$\kappa_e = \frac{\kappa_L \kappa_R}{\kappa_L B_L + \kappa_R B_R} \tag{9b}$$

$$B_e = B_L B_R \tag{9c}$$

$$C_e = B_R C_L + B_L C_R \tag{9d}$$

$$D_e = B_R D_L + B_L D_R \tag{9e}$$

It can be observed that the CS thermal conductivity is no longer based on an arithmetic mean. It is represented by an equivalence thermal conductivity that possesses a harmonic mean of the two elements, thermal conductivities [14]. Derivation for the triangle CS is done analogously and will not be repeated here. Equation (9) is applied in the region where differing material properties are involved.

Φ_D in Eq. (3) is a function of the local diffusion number, C_D. The scheme will automatically switch to full implicit when a degenerate cell, i.e., tetrahedron, pyramid, or prism, is detected within the domain.

$$C_D = \nu \frac{\Delta t}{\Delta X^2} \tag{10a}$$

where Δt is the time step size, ΔX^2 is related to the cell dimension [1], and

$$\nu = \frac{\kappa}{\rho C_P} \tag{10b}$$

One additional time-step constraint has been implemented into the KIVA code to take into account the solid-wall heat conduction mode, and it is based mainly on the Von Neumann stability criterion [15],

$$0 < \Delta t \leq \frac{\Delta X^2}{\nu f} \tag{11a}$$

where

$$\frac{1}{f} = 0.25 \tag{11b}$$

For optimum computation, the time step is set equal to $\Delta X^2 / \nu f$.

The conjugate residual method (CRM) is used as the solver to solve the resulting implicit equation. It will converge within a finite number of steps in addition to having low storage requirement and vectorizable characteristic [16]. The CRM is also the solver used in the KIVA code.

FLUID-SOLID INTERFACE EQUATIONS

The KIVA code uses the law of the wall for both momentum and energy transport near the wall regions. The energy transport is written closely to the expression originally proposed by Launder and Spalding [17]:

$$(q_i'')_R = \frac{(q_i)_R}{|\vec{A}_{i,R}|} = h(T_R - T_i) \tag{12}$$

where

$$h = \frac{\rho_f \nu_l C_p}{\mathrm{Pr}_l} \frac{F}{y}$$

$$F = \begin{cases} \dfrac{R' \ \mathrm{Pr}_l \ \mathrm{RPR}}{1/\kappa - \ln R' + B + 11.05(\mathrm{Pr}_f \ \mathrm{RPR} - 1)} & R' > 11.05 \\ 1.0 & R' < 11.05 \end{cases}$$

$$R' = \frac{c_\mu^{1/4} K^{1/2} y}{\nu_l}$$

Using the quadrilateral CS shown in Figure 1, elements to the left and to the right of the CS are solid and fluid elements, respectively. Subscript i refers to the face center. It should be noted that the fluid solver is based on the multiblock structured method; therefore quadrilateral shape is always assumed at the fluid–solid interface. At the interface the following constraints are used:

$$(T_i)_L = (T_i)_R \tag{13a}$$

$$(q_i'')_L = (q_i'')_R \tag{13b}$$

$$(q_i'')_L = \frac{\kappa_L[B_L(T_i - T_L) + C_L(T_3 - T_1) + D_L(T_4 - T_2)]}{|\vec{A}_{i,L}|} \tag{13c}$$

Solving Eqs. (12), (13), and (8a) for face temperature and face heat flux, one obtains

$$T_i = \frac{\kappa_L(B_L T_L - \mathrm{cross}) + |\vec{A}_{i,L}| h T_R}{\kappa_L B_L + |\vec{A}_{i,L}| h} \tag{14a}$$

$$(q_i'')_R = h_e\left(T_R - T_L + \frac{\text{cross}}{B_L}\right) \tag{14b}$$

where

$$h_e = \frac{\kappa_L B_L h}{\kappa_L B_L + |\vec{A}_{i,L}|h}$$

$$\text{cross} = C_L(T_3 - T_1) + D_L(T_4 - T_2)$$

Heat flux in Eq. (14*b*) is similar to Eq. (12), except for some additional terms. The CS temperature in Eq. (12) is replaced by a summation of the solid-element temperature and cross-diffusion of the solid wall. The convective heat transfer coefficient is also replaced by an equivalent convective heat transfer that accounts for solid wall thermal conductivity.

The KIVA code uses the Monte Carlo method and stochastic particle technique to describe evaporating fuel liquid sprays [1]. Each computational particle represents a number of droplets of identical size, velocity, and temperature. When the spray model is used, spray impingement could occur, forming a wall film. The code currently adopts a particle wall film model, in that the wall film transport is calculated by tracking each computational particle [18, 19]. The model assumes a piecewise-linear temperature profile across the wall film thickness, and it has been modified to take into account the solid wall heat conduction mode; see Figure 2. At the liquid wall film–solid interface the following constraints are used:

$$(T_i)_L = (T_i)_R \tag{15a}$$

$$(q_i'')_L = (q_i'')_p \tag{15b}$$

$$(q_i'')_L = \frac{\kappa_L[B_L(T_i - T_L) + C_L(T_3 - T_1) + D_L(T_4 - T_2)]}{|\vec{A}_{i,L}|} \tag{15c}$$

$$(q_i'')_p = \lambda_\ell(T_p^n)\frac{T_p^{n+1} - T_i}{h_\alpha/2} \tag{15d}$$

where h_α is liquid wall film thickness on cell face α and $\lambda_\ell(T_p^n)$ is the thermal conductivity (temperature dependent) of the liquid wall film. Solving Eq. (15*b*) for face

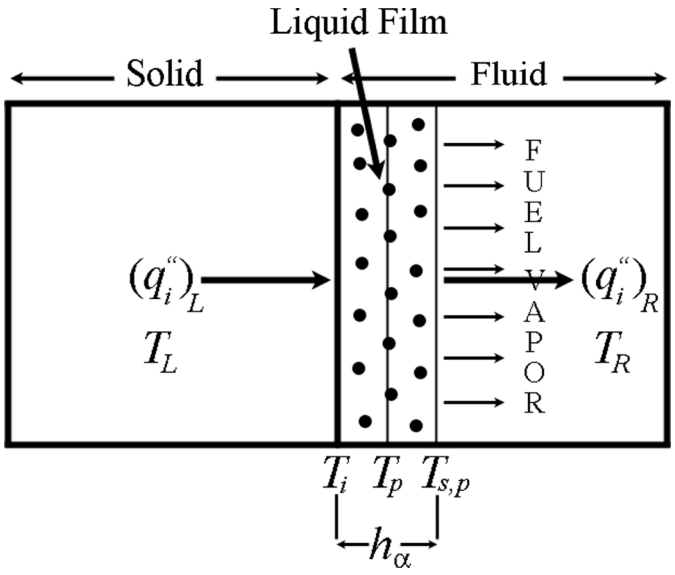

Figure 2. Energy balance at liquid–solid interface.

temperature, one obtains

$$T_i = \frac{\kappa_L/|\vec{A}_{i,L}|[B_L T_L - C_L(T_3 - T_1) - D_L(T_4 - T_2)] + [2\lambda_\ell(T_p^n)/h_\alpha]\ T_p^{n+1}}{(\kappa_L/|\vec{A}_{i,L}|)B_L + [2\lambda_\ell(T_p^n)/h_\alpha]} \tag{16}$$

It should be noted that Eq. (15*d*) is calculated for one particle associated with face α. The total heat flux between the liquid wall film and the solid wall on cell face α is obtained by simple ensemble averaging:

$$(q_i'')_L = \frac{\sum_m [\lambda_\ell(T_p^n)T_p^{n+1} - T_i/h_\alpha - 2]_m}{m} \tag{17}$$

where the summation is performed over all particles m on cell face α.

VALIDATION

Consider 1-D unsteady heat conduction in three cylindrical layers with different thermal-physical properties as shown in Figure 3 and Table 1. The cylinder is initially at a uniform temperature of 300 K. Boundary conditions and geometric specification are as follows

$$r = r_{\text{inner}} \qquad q''_{\text{inner}} = h_{\text{inner}}(T_{\text{inner}} - T_\infty)$$

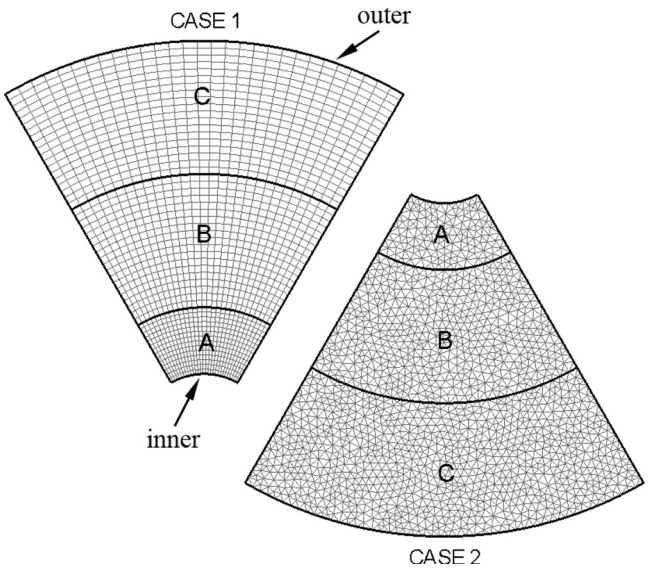

Figure 3. Two cases of 1-D heat conduction.

$$r = r_{\text{outer}} \qquad q''_{\text{outer}} = h_{\text{outer}}(T_{\text{outer}} - T_\infty)$$

$$T_\infty = 500\,\text{K}$$

$$h_{\text{inner}} = 3,540\,\text{W/m}^2\,\text{K}$$

$$h_{\text{outer}} = 7,080\,\text{W/m}^2\,\text{K}$$

Two cases were tested using different element types as shown in Figure 3. Case 1 used pure hexahedron elements, whereas case 2 used pure tetrahedron elements. Periodic-in and-out conditions were imposed on the azimuthal faces to ensure a 1-D problem. As shown in Figure 4, both numerical solutions agree with the exact solution very well. Other validations and case studies can be found in [5] and will not be repeated here.

Table 1. Material properties and geometric specification

Material	A	B	C
r_{inner} (cm)	5	10	20
r_{outer} (cm)	10	20	30
ρ (kg/m^3)	2,770	2,423.75	1,077.22
κ (W/m K)	177	708	708
C_P (J/kg K)	875	1,000	1,000

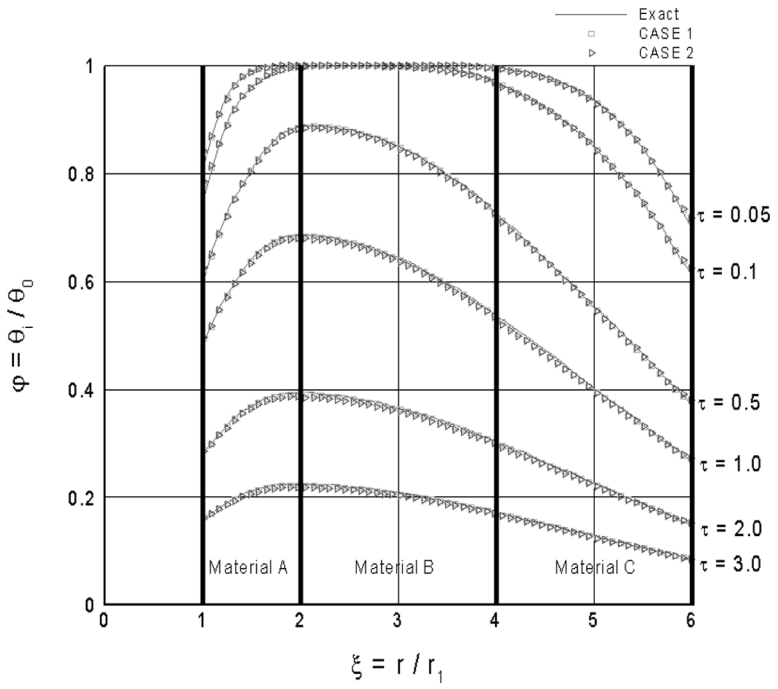

Figure 4. Solution of 1-D heat conduction.

EFFECT OF EQUIVALENT COEFFICIENTS

To investigate the effect of equivalent coefficients in Eq. (9), consider 1-D steady-state heat conduction in a rectangular slab. Two cases were tested: case 1, with equivalent coefficients (EC); and case 2, without EC. Boundary conditions and geometric specifications are given in Figure 5. Numerical solution for case 1 matches the exact solution very well, as shown in Figure 6. It can be observed in Figure 6*b* that in the large-temperature-gradient region, $0 \leq z \leq 5$ cm, case 2 fails to resolve the temperature distribution. About 16 K temperature difference between case 2 and exact solutions can be observed in this region.

ENGINE HEAT TRANSFER STUDY

One of the cylinders of the Ford F-150 5.4-L V8 engine was modeled and is shown in Figure 7. The computational mesh was generated using GRIDGEN [20] software and a modified version of the K3Prep [3] for patching and boundary conditions assignment. The solid mesh was constructed of three elements, tetrahedron, hexahedron, and pyramid, to form a hybrid mesh. The generated mesh has about 106,552 fluid cells and 685,398 solid cells. The engine was assumed to operate at full load. Inlet pressure is maintained at 79,925 Pa and exhaust pressure at 110,000 Pa. Fluid was initially at rest and at standard temperature and pressure (STP) conditions. A summary of engine dimensions and operating conditions is given in Table 2.

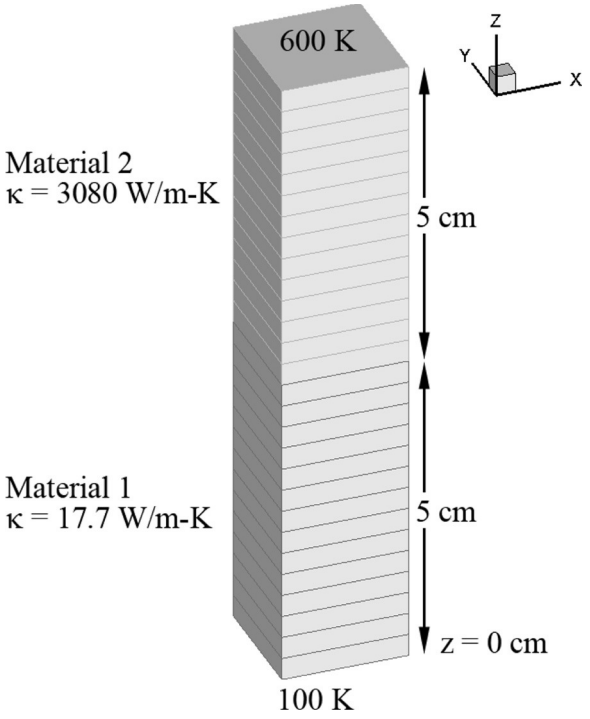

Figure 5. Steady-state heat conduction computational mesh.

At 15° crank angle after top dead center during the intake stroke, a half-sine wave injection pulse injected the liquid gasoline (C_8H_{17}) fuel into the intake port. Ignition started at 18° crank angle before top dead center. The engine metal components were initially at a uniform temperature of 410 K. An adiabatic wall was assumed on all boundary conditions of the solid domain. By default, the code applies the specified constant wall temperature boundary (410 K) to the fluid domain in which the wall boundary is not participating in the conjugate heat transfer calculation; see Figure 7*b* (portion of intake and exhaust ports). Aluminum alloy 2024-T6 was assigned to both the engine head and piston, and iron (99.75% pure) to the engine block [21]. Head gasket material and heating effect from viscous friction between the piston ring and oil film were not included in this study. Since this study focuses on the investigation of the wall heat transfer for the first few engine cycles, it is good to assume no heat loss due to coolant flow or cooling circuit. It would require, depending on the thermal properties of the metal, more engine cycles for the wall heat transfer from the combustion chamber surface to be significantly felt by the cooling circuit. The crevice region, the gap between the piston skirt and cylinder wall, was not modeled. It should be noted that the code will not model temperature distribution inside the valve; therefore, significant heat transfer, especially from the exhaust valve to its seat as they come into contact with each other [22], will be neglected. Two cases were run: case 1, engine simulation with conjugate heat

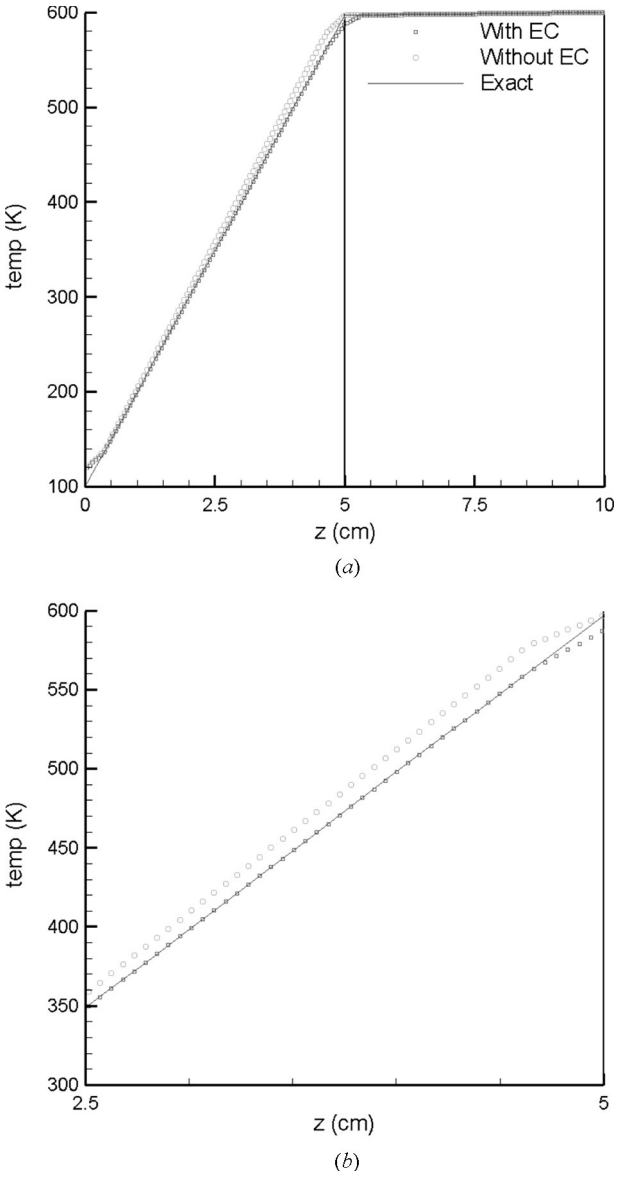

Figure 6. Steady-state heat conduction numerical solution.

transfer mode, coupling gas and solid phases together; and case 2, engine simulation without conjugate heat transfer mode, solving the gas phase alone with a prescribed constant wall temperature of 410 K. Each case was successfully run for four engine cycles (0–2,880 crank angles). Computation for case 1 was performed on a 3.06-GHz Intel Pentium PC machine with 2 GB of RAM, while for case 2 it was performed on a 2.4-GHz AMD Athlon64 4000+ PC machine with 1 GB of RAM. Approximately 15 μs/cycle-cell of CPU time was recorded for case 1.

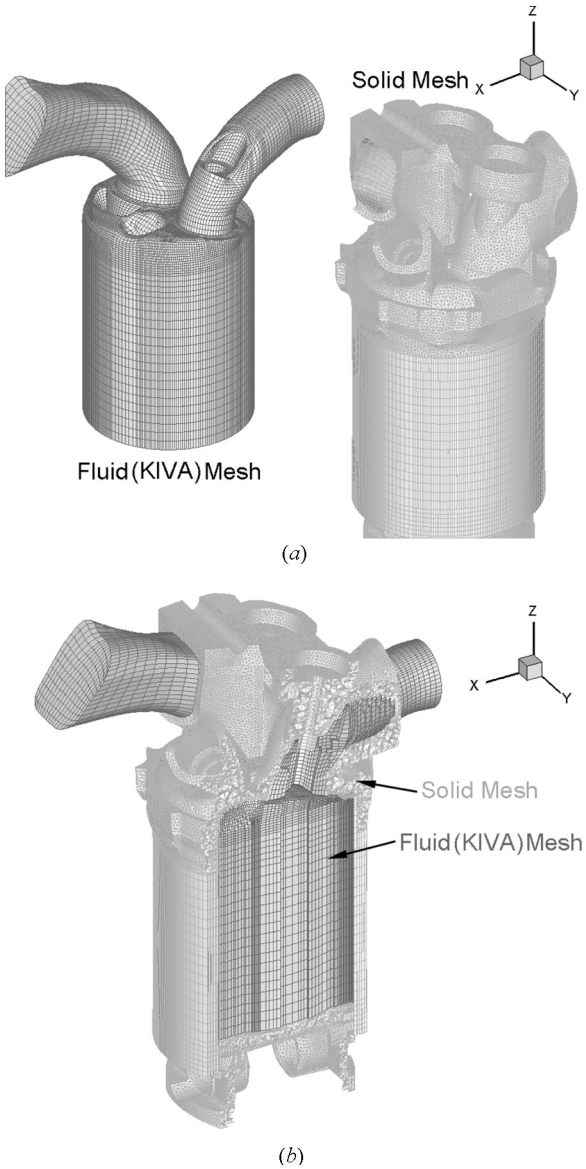

Figure 7. Engine mesh.

Table 2. Ford engine specifications

Cylinder bore × stroke	9.017 cm × 10.58 cm
Connecting rod length	16.91 cm
Compression ratio	9.09
Injected fuel per cycle	.047 g (gasoline)
RPM	1,800

The in-cylinder mixture mass in the second engine cycle was reduced by 9% as a result of the specified initial conditions and the remaining products of combustion from the previous cycle; see Figure 8. This variation shifts both the in-cylinder peak pressure and temperature in time; see Figure 9. Figure 10 shows area-averaged cylinder head heat flux for both cases. The peak of the area-averaged cylinder head heat flux of case 1 in the first engine cycle is about $480\,W/cm^2$, $50\,W/cm^2$ higher than the second, third, and fourth engine cycles. It was observed that the gas motion inside the combustion chamber increased when the exhaust valve opened, which resulted a significant increase in heat transfer rate to the cylinder head.

During the period of liquid droplets impinging on the solid wall, it was interesting to note that the computation for case 2 always encountered problems related to the source term due to the spray in the transport energy equation of the gas phase, while case 1 did not. By default the KIVA code will restart the computation with halved time-step size. Thus case 2 requires 300 more cycles than case 1 to complete an engine cycle (two revolutions). It should be noted that the energy transport of the wall film model in the KIVA code is solved by an iterative method. When the total number of iterations exceeds 50 (maximum allowable number of iterations), new wall film temperature will be updated with its latest iterated value. This is done to increase overall computational efficiency since the physics of the wall film is considered less important for most engine applications (ideally, one wants to reduce the time-step size or increase the allowable number of iterations). After a number of cycles, the numerical errors could grow and could result in the halved-time-step problem. On the other hand, when the conjugate heat transfer model was used,

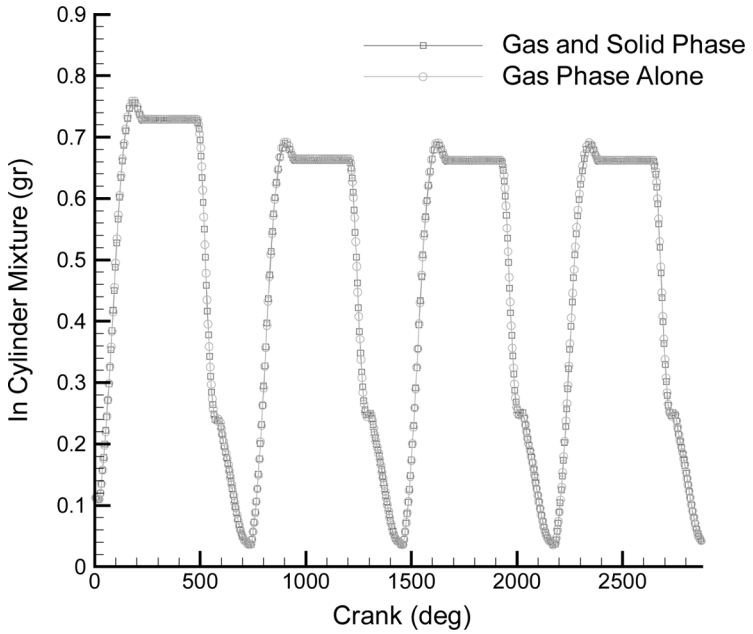

Figure 8. In-cylinder mixture mass.

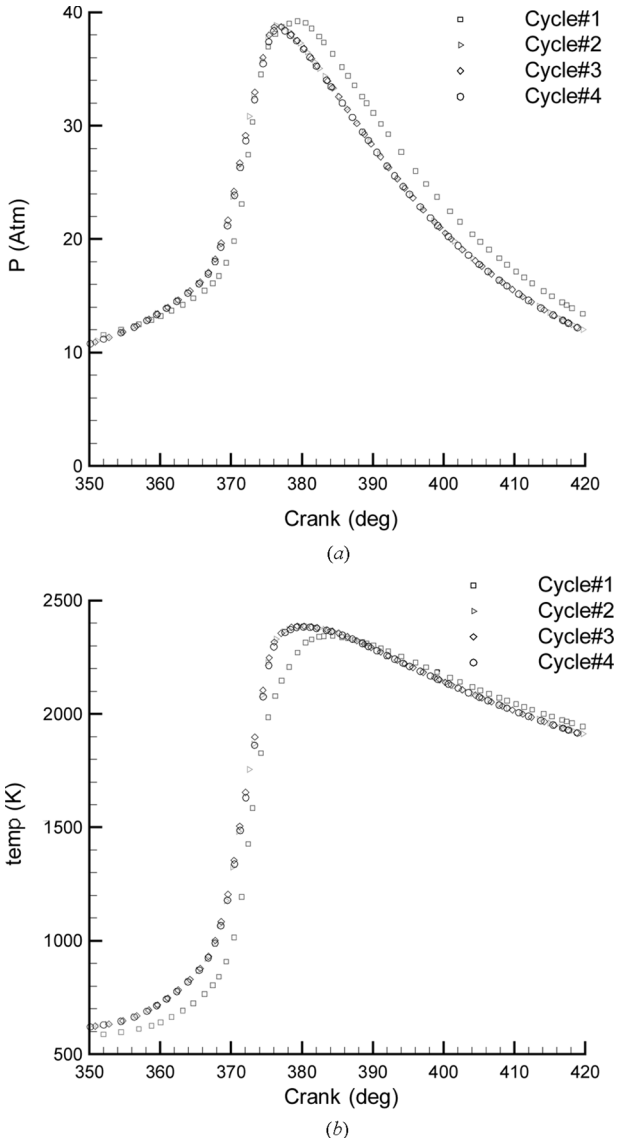

Figure 9. In-cylinder gas pressure and temperature (case 1).

the numerical errors generated were partially absorbed, resulting in a more stable computation.

It was interesting to note that in-cylinder fuel vapor mass in case 1 is always lower than the fuel vapor mass in case 2 during the intake stroke. This could be the result of the lower temperature of the intake port wall in case 1. Over a period of time, the wall cools down as a result of the thermal interaction between the liquid wall film and the intake port wall. This could potentially lower the wall film

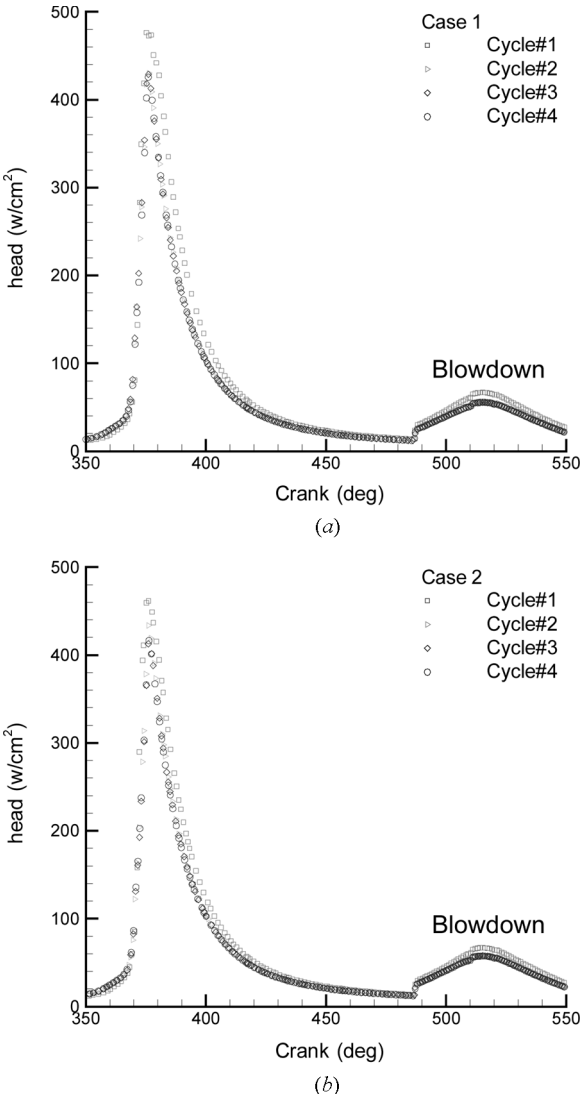

Figure 10. Cylinder head heat flux (area-averaged).

vaporization rate for the next engine cycle. On the other hand, wall temperature in case 2 is always constant, which results in a constant fuel vaporization rate. Another interesting observation reveals that all liquid spray in case 1 is completely vaporized about 24 crank angles faster than in case 2. This is because of the increasing combustion chamber wall temperature in case 1 as opposed to the constant wall temperature in case 2. In-cylinder pressure and temperature for the two cases are about the same for all four engine cycles, which indicates a small influence of the wall temperature change on the thermodynamic properties of the gas.

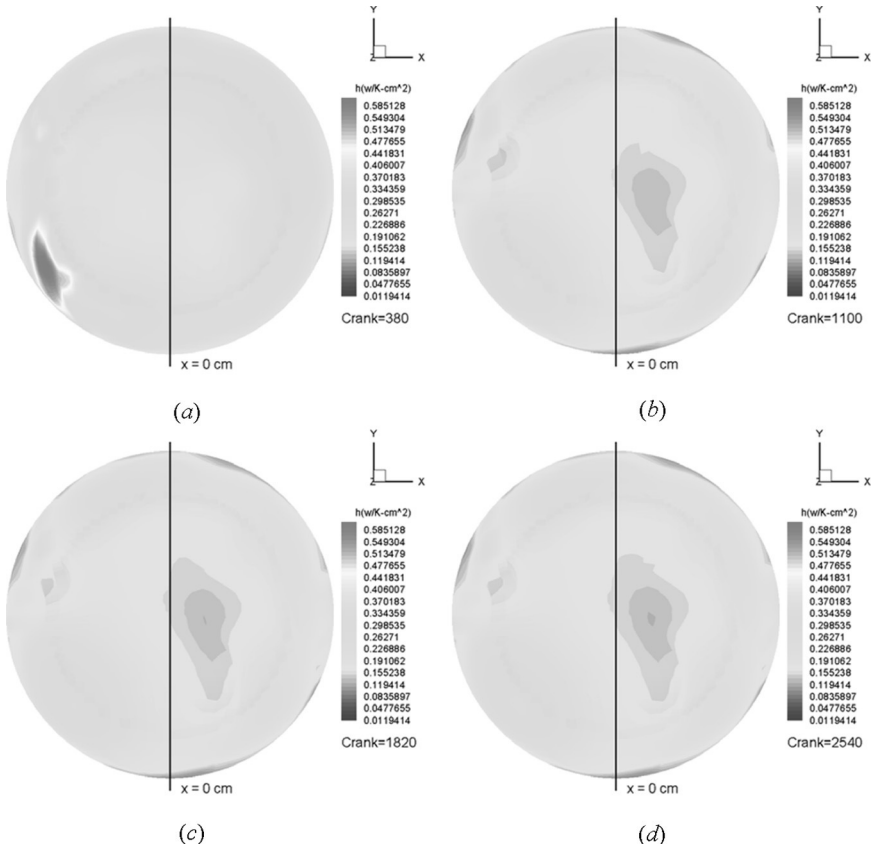

Figure 11. Near-wall gas convective heat transfer coefficient (piston crown).

To predict hotspots, one must run the computation for many engine cycles, and this is obviously impossible to accomplish, as described in the introduction. Using heat flux history, $q''_w(\vec{x}, t)$, compiled from the case 1 study is considered to be a sensible approach, under the assumption that both the gas flow and combustion intensity behave in a periodic manner or vary slowly between engine cycles. If indeed the assumption is acceptable, the wall heat flux is still expected to vary slowly in response to the wall temperature change. To include the transient wall temperature effect, one could instead use the history of two variables: near-wall fluid temperature $T_f(\vec{x}, t)$ and near-wall fluid convective heat transfer coefficient $h(\vec{x}, t)$. Since the convective heat transfer coefficient is a strong function of fluid velocity, under the above assumption, periodic behavior of this variable is assumed. Near-wall gas temperature is influenced by the local wall temperature and nearby gas temperature, but its effect is assumed to be small.

To investigate the above claims, the two variables were recorded during the computation, starting from 0 to 2,880 crank angles. Near-wall (piston crown surface) fluid convective heat transfer coefficient and temperature are shown in Figures 11 and 12. It can be observed that both variables at the last three engine

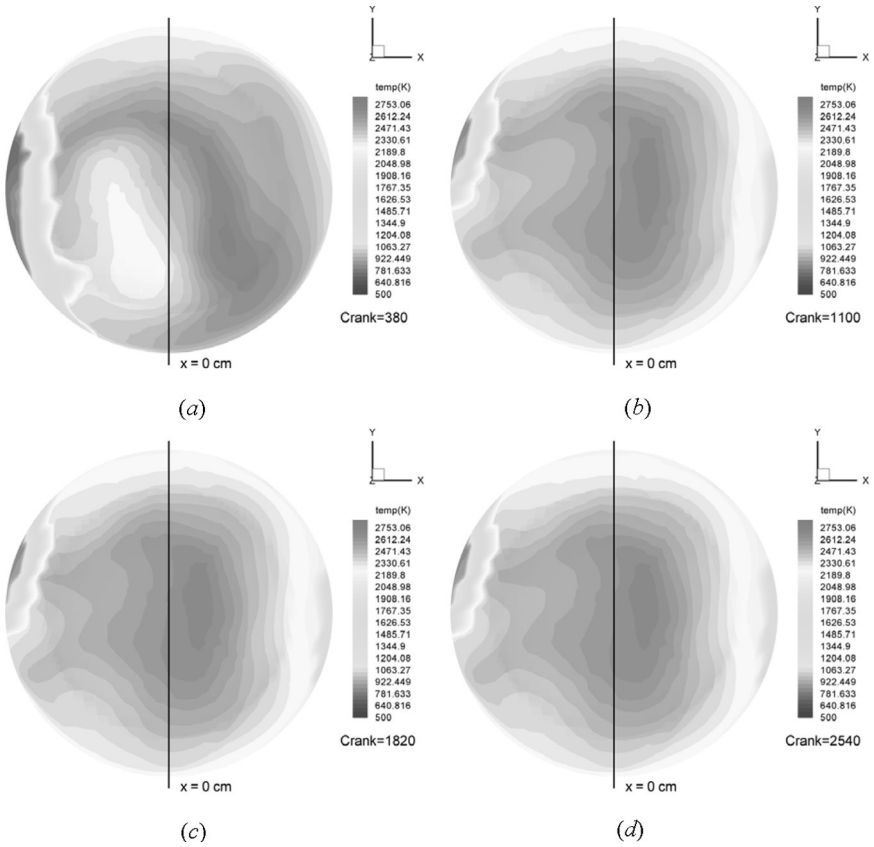

Figure 12. Near-wall gas temperature (piston crown).

cycles have similar contour profiles. To see more detail, values of the two variables are plotted along the $x = 0\,\text{cm}$ line, shown in Figure 13. The line follows the shape of the piston crown (the z coordinate is not constant), which has a scallop shape. Again a very small deviation for the convective heat transfer coefficient after the first engine cycle and fairly small deviation for the near-wall gas temperature after the second engine cycle can be observed, indicating a periodic behavior. The increasing wall temperature in case 1, as the time advances, does not strongly influence the near-wall gas temperature, which proves one of the above claims (the near-wall gas temperature should be weakly affected by the local wall and nearby gas temperatures). Temperature trace on the cylinder wall and on the intake port wall, as a result of cooling effect of the liquid wall film during the intake stroke, can be observed in Figure 14. It should be noted that the color band used in Figure 14 captures the maximum and minimum temperature of all four figures. The liquid wall film at four different occurrences formed approximately on the same surface, which was an indication of the periodic behavior.

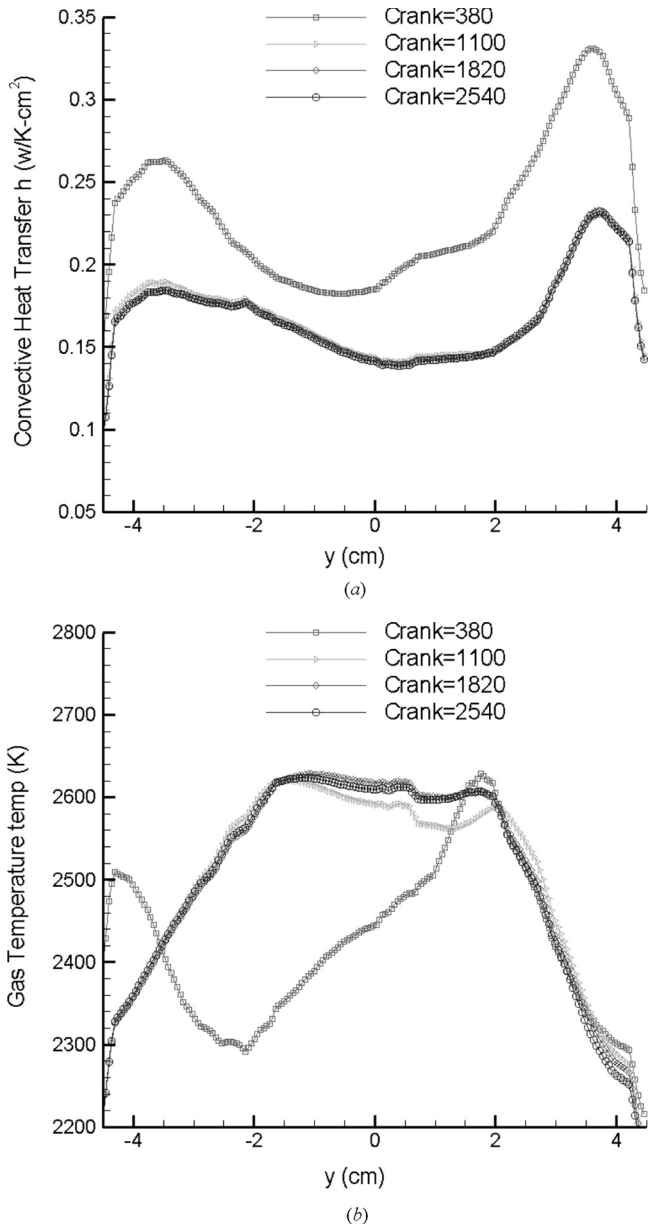

Figure 13. Fluid properties along $x = 0$ cm line (case 1).

CONCLUSION

A conjugate heat transfer model has been successfully implemented into the KIVA code. The numerical model to solve the heat conduction equation is based on an unstructured finite-volume method, which provides flexibility for modeling

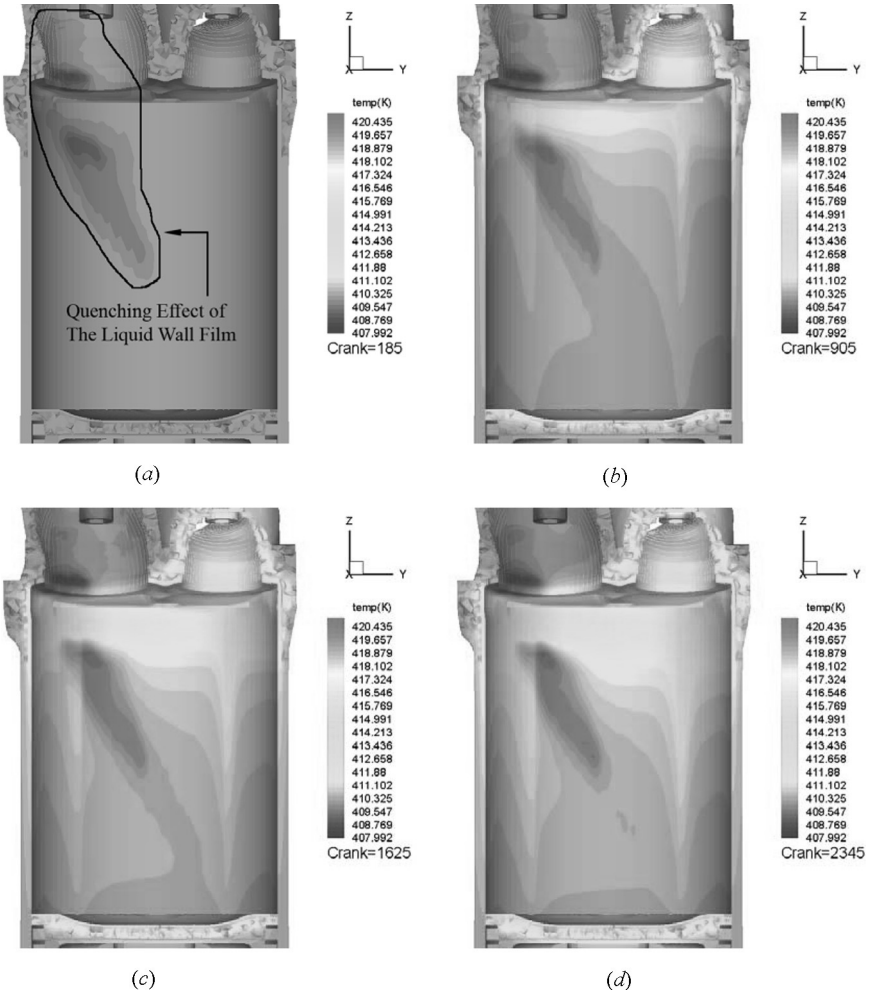

Figure 14. Cooling effect of fuel liquid film.

complex geometry, especially in the cylinder head region. The current scheme is compatible with the to-be-released unstructured KIVA 4 code [23, 24]. Comparison of the heat conduction model with exact solutions was performed and validated. The validation also shows the model is capable of solving transient heat conduction problems with a multiple-medium domain, e.g., a sandwich arrangement of cast-iron engine block, head gasket, and aluminum-alloy engine head. The code can be used as a tool to locate engine hotspots. To predict hotspot magnitude accurately, one must consider some important aspects of engine heat transfer, e.g., mixing model, turbulence model, coolant boiling model, mechanical friction, fluctuating ambient environment inside the crank case, etc.

The model can be used to better understand hydrocarbon emissions from the thermal interaction between fuel liquid film and the combustion chamber wall during

cold start. Since the code is not able to model temperature distribution inside the valves, further improvement to the code can still be made.

A transient 3-D heat flux history on the combustion chamber surface can be obtained by running the code with conjugate heat transfer mode. It can then be used as a transient 3-D thermal boundary condition for solving the heat conduction equation alone. Two approaches can be used as the transient thermal boundary: (1) heat flux history $q''_w(\vec{x}, t)$ and (2) near-wall gas property history, $h(\vec{x}, t)$ and $T_f(\vec{x}, t)$. In the second approach, the wall heat flux is allowed to vary due to the change of the wall temperature; thus it is considered to be more realistic. These data should be compiled using the second or the third engine cycle, when fluid solution dependency to its initial condition is considered weak.

When the conjugate heat transfer model was not in use and when the liquid droplets impinged on the solid wall to form a wall film, the computation had to reduce the time-step size to avoid negative internal energy in the gas phase, which resulted in an additional number of cycles to complete the computation. On the other hand, running the calculation with the conjugate heat transfer mode resulted in better thermal coupling of the fluid mixtures, fuel liquid film, and the solid wall. There was no reduction in time-step size during the period in which the liquid droplets formed a wall film.

REFERENCES

1. A. A. Amsden, P. J. O'Rourke, and T. D. Butler, KIVA-II: A Computer Program for Chemically Reactive Flows with Sprays, Los Alamos Natl. Lab. Rep. LA-11560-MS, Los Alamos, NM, 1989.
2. A. A. Amsden, KIVA-3: A KIVA Program with Block-Structured Mesh for Complex Geometries, Los Alamos Natl. Lab. Rep. LA-12503-MS, Los Alamos, NM, 1993.
3. A. A. Amsden, KIVA-3V: A Block-Structured KIVA Program for Engines with Vertical or Canted Valves, Los Alamos Natl. Lab. Rep. LA-13313-MS, Los Alamos, NM, 1997.
4. A. A. Amsden, KIVA-3V, Release 2, Improvements to KIVA-3V, Los Alamos Natl. Lab. Rep. LA-13608-MS, Los Alamos, NM, 1999.
5. E. Urip, K. H. Liew, S. L. Yang, and O. Arici, Numerical Investigation of Heat Conduction with Unsteady Thermal Boundary Conditions for Internal Combustion Engine Application, *Heat Transfer 2004: Proc. 2004 ASME Int. Mechanical Engineering Congress and Exposition*, California, 2004.
6. Y. Liu and R. D. Reitz, Modeling of Heat Conduction within Chamber Walls for Multidimensional Internal Combustion Engine Simulation, *Int. J. Heat Mass Transfer*, vol. 41, pp. 859–869, 1998.
7. J. F. Wiedenhoefer and R. D. Reitz, Modeling the Effect of EGR and Multiple Injection Schemes on I.C. Engine Component Temperatures, *Numer. Heat Transfer A*, vol. 37, pp. 673–694, 2000.
8. A. P. Kleemann, P. Menegazzi, and S. Henriot, Numerical Study on Knock for an SI Engine by Thermally Coupling Combustion Chamber and Cooling Circuit Simulations, SAE Technical Paper 2003-01-0563, 2003.
9. A. D. Blank, Conjugate Conduction-Convection Heat Transfer Model for the Valve Flow-Field Region of Four-Stroke Piston Engines, *Numer. Heat Transfer A*, vol. 18, pp. 283–308, 1990.
10. C. P. Chiu and Y. S. Kuo, Study of Turbulent Heat Transfer in Reciprocating Engine Using an Algebraic Grid Generation Technique, *Numer. Heat Transfer A*, vol. 27, pp. 255–271, 1995.

11. A. G. Catto and A. T. Prata, A Numerical Study of Instantaneous Heat Transfer During Compression and Expansion in Piston-Cylinder Geometry, *Numer. Heat Transfer A*, vol. 38, pp. 281–303, 2000.
12. D. B. Spalding and N. H. Afgan, *Heat and Mass Transfer in Gasoline and Diesel Engines*, pp. 17–19, Hemisphere, New York, 1989.
13. Y. G. Lai (CFD Research Corp), H. Nguyen, and J. J. Lee, Coupled Thermofluid Analysis Method with Application to Thermodynamic Vent Systems, *J. Thermophys. Heat Transfer*, vol. 9, pp. 278–284, 1995.
14. S. V. Patankar, *Numerical Heat Transfer and Fluid Flow*, pp. 44–47, Hemisphere, New York, 1980.
15. K. A. Hoffmann and S. T. Chiang, *Computational Fluid Dynamics*, 4th ed., pp. 113–148, Engineering Education System, Kansas, 2000.
16. P. J. O'Rourke and A. A. Amsden, Implementation of a Conjugate Residual Iteration in the KIVA Computer Program, Los Alamos Natl. Lab. Rep. LA-10849-MS, Los Alamos, NM, 1986.
17. B. E. Launder and D. B. Spalding, *Comput. Meth. Appl. Mech. Eng.*, vol. 3, p. 269, 1974.
18. P. J. O'Rourke and A. A. Amsden, A Particle Numerical Model for Wall Film Dynamics in Port-Injected Engines, SAE Technical Paper 961961, 1996.
19. P. J. O'Rourke and A. A. Amsden, A Spray/Wall Interaction Submodel for the KIVA-3 Wall Film Model, SAE Technical Paper 2000-01-0271, 2000.
20. Gridgen®, Grid Generation and Pre-Processing for CFD, V.15.07, Pointwise Inc., Fort Worth, TX, USA, 2005.
21. Frank P. Incropera and David P. DeWitt, F*undamentals of Heat and Mass Transfer*, 5th ed., pp. 905–906, Wiley, New York, 2001.
22. M. H. Shojaefard, A. R. Noorpoor, D. A. Bozchaloe, and M. Ghaffarpour, Transient Thermal Analysis of Engine Exhaust Valve, *Numer. Heat Transfer A*, vol. 48, pp. 627–644, 2005.
23. D. J. Torres and P. J. O'Rourke, KIVA-4, 14th Int. Multidimensional Engine Modeling User's Group Meeting, MI, 2004.
24. D. J. Torres, KIVA-4: Validation, Rezoning, and Remapping, 15th Int. Multidimensional Engine Modeling User's Group Meeting, 2005.